Near infrared and ultraviolet spectra of TLEs

F. J. Gordillo-Vázquez,[1] A. Luque,[1] and M. Simek[2]

Received 10 January 2012; revised 19 April 2012; accepted 19 April 2012; published 26 May 2012.

[1] We have found that sprites, beads and halos have similar optical spectra, but measurable differences in the near IR and near UV spectra. In particular, near infrared (NIR) and ultraviolet (UV) spectra of sprites, halos and beads corresponding to the first (1PG) and second positive (2PG) bands of N_2 have been calculated for different observation altitudes from mountains (3.25 km) to airplanes (14 km), balloons (35 km) and space (nadir) platforms. The calculated non-equilibrium vibrational distribution functions (VDF) of the $N_2(B^3\Pi_g)$ states in halos and beads show that the calculated NIR emissions produced through strong N_2-1PG ($B^3\Pi_g \rightarrow A^3\Sigma_u^+$) transitions differ from the calculated sprite spectral emission patterns at ∼888 nm but particularly pronounced differences are found in the NIR spectral region at ∼1046 nm and ∼1231 nm corresponding to the N_2-1PG (0,0) and (0,1) transitions, respectively. The blue - near UV spectra from N_2-2PG ($C^3\Pi_u \rightarrow B^3\Pi_g$) transitions in halos and beads also exhibits slightly different spectral features when compared to the blue - near UV spectrum of sprites for bands originating from higher v-levels ($v > 0$) although they might not be above electronic noise level to be distinguished.

Citation: Gordillo-Vázquez, F. J., A. Luque, and M. Simek (2012), Near infrared and ultraviolet spectra of TLEs, *J. Geophys. Res.*, *117*, A05329, doi:10.1029/2012JA017516.

1. Introduction

[2] Spectral measurements of the N_2-1PG ($B^3\Pi_g \rightarrow A^3\Sigma_u^+$) near infrared (NIR) emissions from Transient Luminous Events (TLEs) can be relevant to clarify the energy deposited in the mesosphere by TLEs. Recent results from the comparison of sprite visible and NIR optical emissions show that the NIR is brightest in the sprite central body, fainter at the tops, and barely above sensitivity in the tendrils [*Siefring et al.*, 2010]. In addition, the comparison performed by *Siefring et al.* [2010] between sprite and OH airglow emissions indicate that the NIR sprite emissions (mainly from the $N_2(B^3\Pi_g)$ 1PG) are extremely bright. According to *Siefring et al.* [2010] the EXL98 campaign NIR and visible sprite emission comparisons imply a change in the central core-to-top brightness ratio in sprites that could be due to a change in the relative vibrational populations of $N_2(B^3\Pi_g)$ involved in the NIR (v = 0, 1; core region) and visible (v = 2, 3,.; top region) emitting regions of sprites. Unfortunately, there have been few spectroscopic campaigns of TLEs since the mid 1990s when the simultaneous works by *Mende et al.* [1995] and *Hampton et al.* [1996] provided the first spectroscopic studies of N_2-1PG sprite emissions at standard video rate in the visible (550 nm–840 nm) electromagnetic spectrum. Later results by *Morrill et al.* [1998] and *Bucsela et al.* [2003] dealt with spectroscopic observations of low altitude sprites at 53 km and 57 km (probably sprite tendrils with very faint NIR emission) that provided preliminary spectral data of the only sprite NIR (up to 900 nm) emission observations existing to date together with a tentative estimation of the relative vibrational population of N_2 ($B^3\Pi_g$, v = 1). However, as acknowledged by the authors, their results were affected by sensitivity calibration errors [*Bucsela et al.*, 2003]. The most recent spectroscopic observations of the $N_2(B^3\Pi_g)$ 1PG sprite emissions at different altitudes (52.7 km–86.4 km) [*Kanmae et al.*, 2007] only covered the visible range (640–820 nm) involving the transitions Δv = 1, 2, 3 of the N_2-1PG but providing no information about the relative vibrational populations of N_2 ($B^3\Pi_g$, v = 1) involved in the strongest sprite NIR emissions related to the Δv = 1, 0, −1, −2 transitions of N_2-1PG.

[3] Presently, the only near UV (250 nm–390 nm) and violet (390–450 nm) spectra of sprites are those shown in the recent work by *Heavner et al.* [2010] that focused on emissions from $N_2(C^3\Pi_u)$ 2PG of sprites at 65 km altitude recorded in the EXL98 aircraft observation campaign in July 1998 using ∼4 nm spectral resolution and 60 fps recording rate. However, the spectrum shown in *Heavner et al.* [2010] was published without correction for instrument spectral response and, consequently, can not be easily compared with synthetic spectra. Regarding spectroscopy of halos, the only available spectral study to date was published by *Wescott et al.* [2001] and it was about the Halo N_2-1PG optical emission in the visible (550 nm–820 nm) recorded back in June 22, 1995 during one of the first spectral campaigns

[1]Instituto de Astrofísica de Andalucía, CSIC, Granada, Spain.
[2]Department of Pulse Plasma Systems, Institute of Plasma Physics v.v.i., Academy of Sciences of the Czech Republic, Prague, Czech Republic.

Corresponding author: A. Luque, Instituto de Astrofísica de Andalucía, CSIC, PO Box 3004, 18080 Granada, Spain. (aluque@iaa.es)

0148-0227/12/2012JA017516

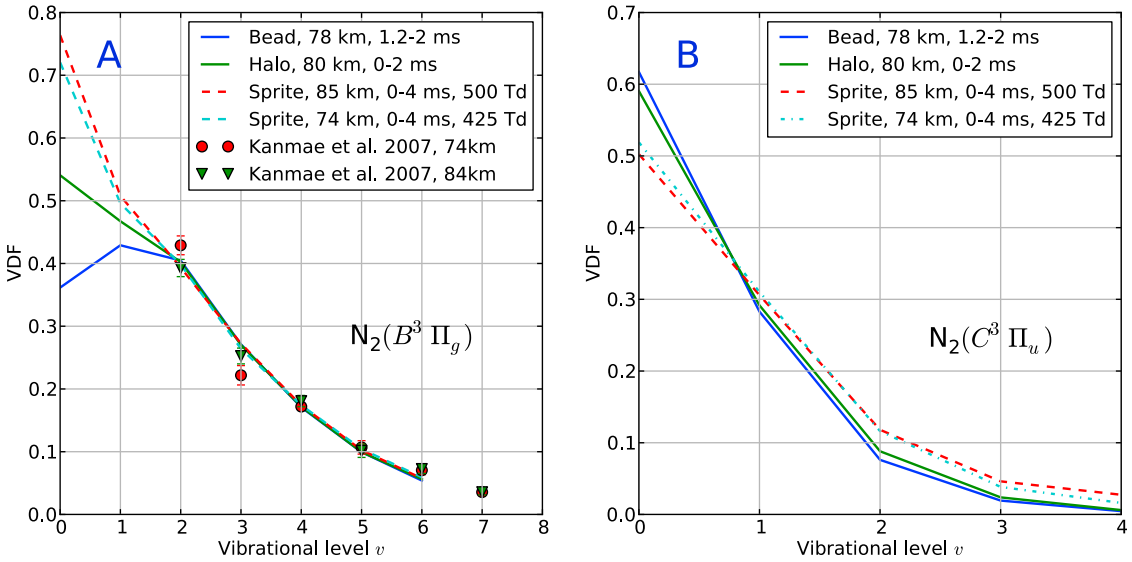

Figure 1. Calculated time integrated VDFs of (a) $N_2(B^3\Pi_g)$ 1PG and (b) $N_2(C^3\Pi_u)$ 2PG corresponding to sprites (at 74 km and 85 km), halos (at 80 km) and sprite beads (at 78 km). The integration times of the calculated VDFs are shown in the figures. For comparison, the VDF of $N_2(B^3\Pi_g, v = 2 - 6)$ in sprites as observed by *Kanmae et al.* [2007] through spectroscopic recording (640–820 nm) using 3 ms temporal resolution and 3 nm spectral resolution is also shown in Figure 1a.

of TLEs [*Hampton et al.*, 1996]. No NUV nor NIR spectra of Halos are available. Similarly, to the author's knowledge, there are no published recorded spectra of sprite beads in any spectral range (UV, visible, NIR).

[4] Here we present calculations of the non-equilibrium VDFs of $N_2(B^3\Pi_g)$ 1PG and $N_2(C^3\Pi_u)$ 2PG corresponding to sprites, halos and sprite beads. The calculated VDFs have allowed us to generate synthetic spectra of sprites (74 km and 85 km), halos (80 km) and sprite beads (78 km) covering the NIR (up to 1300 nm), visible (450 nm–750 nm) and near UV - violet (250 nm–450 nm) spectral ranges. We have found that the calculated $N_2(B^3\Pi_g)$ VDFs of sprites, halos and sprite beads are significantly different for $v = 1$ and, especially, for $v = 0$, where NIR emissions are important. Besides this, our calculated VDFs of $N_2(B^3\Pi_g)$ agree quite well [*Gordillo-Vázquez*, 2010; *Luque and Gordillo-Vázquez*, 2011b] with the measured sprite VDFs of the N_2-1PG visible spectrum (including the transitions $\Delta v = 1, 2, 3$) recorded by *Kanmae et al.* [2007]. In consequence, our results indicate that, while visible spectra are quite the same, the calculated NIR spectra of sprites, halos and sprite beads exhibit significant differences that could be above sensitivity and, consequently, detectable, in the (0,1) (888.3 nm), (0,0) (1046 nm) and (0,1) (1231 nm) bands. Finally, our calculations also predict different spectral features in the $N_2(C^3\Pi_u)$ 2PG near UV emissions from sprites, halos and sprite beads corresponding to bands originating from higher vibrational numbers $v > 0$ that could be detected from balloons (35 km) and/or space platforms.

2. Model and Spectra Calculations

[5] We use the air plasma kinetic model described in *Gordillo-Vázquez* [2008] and *Gordillo-Vázquez* [2010]: a zero-dimensional model that solves a set of differential rate equations for each of the different species considered (electrons, ions, atoms and molecules) and each of the electronically and vibrationally excited species in the streamer, halo and bead air plasma coupled to a time-dependent Boltzmann equation for the electron energy distribution function with a prescribed time-dependent electric field. In this model, all the kinetics are self-consistent, although the electrodynamics are not consistently solved with the plasma kinetics since the Poisson equation is not considered. In this regard, it has been assumed that the time-dependent reduced electric field (E/N, where N is the gas density at a given altitude), within sprite streamers, sprite halo and bead air plasmas is an external parametric function that is calculated off line. For sprite streamers, we assume a pulse-like shape of 500 Td with a duration of 5μs [*Gordillo-Vázquez*, 2008], whereas for sprite halos and beads we used the density dependent model described in *Luque and Ebert* [2009, 2010] where electrons diffuse and drift in the local electric field with an altitude-dependent mobility. We consider halos as due to quasi-electrostatic fields from lightning as originally proposed by *Barrington-Leigh et al.* [2001]. The details on the calculation of the profile of the reduced electric fields causing sprite beads and halos at ~80 km were described in *Luque and Gordillo-Vázquez* [2011a] and *Gordillo-Vázquez et al.* [2011], respectively. The modeled field for a halo lasts about 2 ms, peaking at 154 Td. To model bead emissions we used an electric field resulting from the passage of a streamer head followed by a field of about 70 Td, lasting about 1 ms [*Luque and Gordillo-Vázquez*, 2011a]; to calculate the vibrational populations and emitted spectra we removed from the time integration the passage of the streamer head.

[6] The kinetic model [*Gordillo-Vázquez*, 2008, 2010] that is used here to calculate the non-equilibrium vibrational kinetics of air plasmas generated by sprite streamers, halos and beads incorporates the improved set of $N_2(B^3\Pi_g, v)$ and $N_2(C^3\Pi_u, v)$ quenching rates, and the N_2 $(a^1\Pi_g, v)$ and NO

Table 1. Relative Proportion Between the Calculated Sprite Halo-Bead Time-Integrated Vibrational Populations

	$N_2(B^3\Pi_g, v)_{bead}$ / $N_2(B^3\Pi_g, v)_{sprite}$	$N_2(B^3\Pi_g, v)_{sprite}$ / $N_2(B^3\Pi_g, v)_{halo}$
v = 0	2.21	1.76
v = 1	3.80	1.40
v = 2	4.45	1.31
v > 2	4.38	1.32

($A^2\Sigma^+$), NO($C^2\Pi_r$) and NO($B^2\Pi$) kinetics recently described in *Luque and Gordillo-Vázquez* [2011b] and *Gordillo-Vázquez et al.* [2011], respectively. In addition to this, our kinetic model for TLEs includes the mechanism of associative detachment that releases electrons from O^- when reacting with N_2 to generate N_2O [*Gordillo-Vázquez and Luque*, 2010; *Luque and Gordillo-Vázquez*, 2012].

[7] Following the approach described in *Gordillo-Vázquez et al.* [2011] we have calculated synthetic emission spectra of sprite streamers, halos and beads associated to their NUV and NIR optical emissions. To model the emission of the 1PG and 2PG systems of the neutral N_2, we applied an approach based on calculating all allowed transitions between rotational manifolds of the upper and lower vibronic states arranged in a sequence of bands [*Simek et al.*, 1995; *Simek*, 2002]. Here we considered all allowed rotational transitions between $N_2(C^3\Pi_u, v = 0-4)$ and $N_2(B^3\Pi_g, v = 0-12)$, and between $N_2(B^3\Pi_g, v = 0-12)$ and $N_2(A^3\Sigma_u^+, v = 0-20)$. After creating band profiles for all bands of a given system, we composed the complete spectrum of the 1PG and 2PG systems for the VDFs obtained by the kinetic modeling using the Einstein coefficients given by *Gilmore et al.* [1992]. All bands were modeled assuming a Boltzmann rotational temperatures of T_R = 220 K convolved with triangular line-shapes corresponding to resolutions of $\Delta\lambda$ = 3 nm and $\Delta\lambda$ = 3.5 nm for the 1PG and 2PG systems of N_2, respectively. The NUV and NIR synthetic spectra for sprite streamers, halos and beads were calculated for mountain (3.25 km), aircraft (14 km), balloon (35 km) and nadir-viewing space observation platforms (full transmission), using MODTRAN [*Anderson et al.*, 1993] as the atmospheric transmission model with a source altitude at 80 km.

3. Results

[8] Figure 1 shows the calculated VDFs of $N_2(B^3\Pi_g)$ 1PG and $N_2(C^3\Pi_u)$ 2PG corresponding to sprites (at 74 km and 85 km), halos (at 80 km) and sprite beads (at 78 km). The data corresponding to the observed VDFs of $N_2(B^3\Pi_g)$ 1PG at 72.7–75.0 km and 84.4–86.4 km as reported by *Kanmae et al.* [2007] are also included in Figure 1. The VDFs represent population densities of vibrational levels relative to the total density of the considered electronic state; i.e. they normalize such that the sum of the values of each vibrational level equals one. This is the case for the VDF of $N_2(C^3\Pi_u)$. However, for the VDF of $N_2(B^3\Pi_g)$, only levels with $v = 2$ to $v = 6$ are included in the normalization in order to compare with available observations by *Kanmae et al.* [2007].

[9] As can be seen in Figure 1a, sprite, halo and sprite bead 1PG N_2 VDFs are quite similar from $v = 2$ through $v = 6$, which explains the similarity detected between sprite and halo spectral features in the visible (640 nm–840 nm) region of the 1PG N_2 band emissions [*Wescott et al.*, 2001; *Kanmae et al.*, 2007; *Gordillo-Vázquez et al.*, 2011]. No sprite bead spectral observations are published to date though, according to Figure 1a, bead optical emissions corresponding to the $N_2(B^3\Pi_g)$ 1PG visible spectral range should exhibit quite similar (or the same) spectroscopic features to those of sprites and halos. However, according to Figure 1a, there is a difference (between the 1PG N_2 VDFs of sprites, halos and beads) in the $v = 1$ level and, especially,

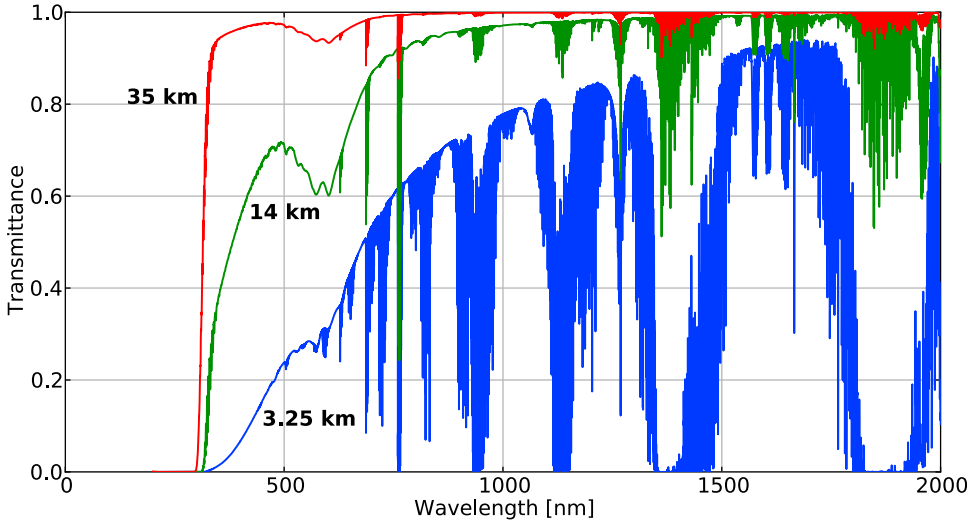

Figure 2. Atmospheric light transmittance using MODTRAN predictions [*Anderson et al.*, 1993] between 250 nm and 2000 nm. The cases shown correspond to light transmittances through 500 km atmospheric path length reaching observers in mountains (3.25 km), airplanes (14 km) and balloons (35 km). Absorption due to H_2O molecules starts to be important in the near infrared (NIR) spectral region from 850 nm and beyond. The source altitude considered for all the cases was 80 km. Full transmittance (1) is the case assumed for an observer in a space platform.

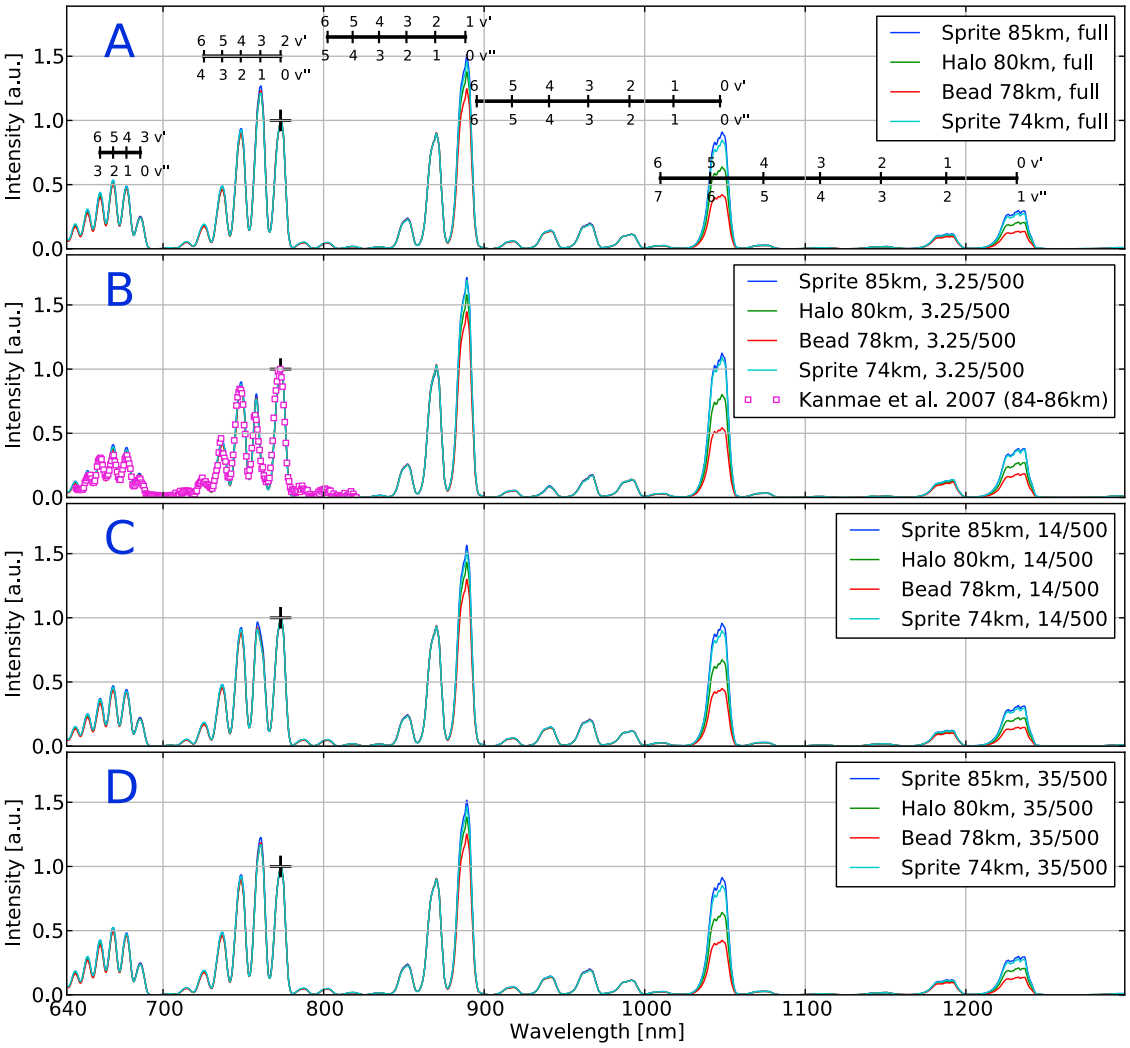

Figure 3. (a) Calculated spectra of the 1PG N_2 from 640 nm to 1300 nm without correction for atmospheric transmittance, (b) corrected for atmospheric transmittance assuming 500 km atmospheric path length from observers in mountains (3.25 km), (c) airplanes (14 km), and (d) balloons (35 km). The spectrum from space (nadir) platforms at 400 km altitude is the same as that shown in Figure 3a. The spectra were calculated for a gas temperature of 220 K and a spectral resolution of $\Delta\lambda = 3$ nm. The normalization of the spectra was done with respect to the (2,0) transition at 773.2 nm. For comparison, the spectrum of sprites as observed by *Kanmae et al.* [2007] from Langmuir Observatory (3.25 km altitude) through spectroscopic recording (640–820 nm) with 3 ms and 3 nm temporal and spectral resolution, respectively, is also shown in Figure 3b. Note that the word *full* in Figure 3a stands for full transmittance.

in the $v = 0$ level where the normalized sprite bead vibrational population is approximately half that of sprites and 30% lower than that of halos. This change in the relative vibrational populations of $N_2(B^3\Pi_g)$ involved in the NIR ($v = 0$, 1; core sprite region) and visible ($v = 2$, 3,.; top sprite region) emitting sprite regions can be the underlying reason that explains the change in the central core-to-top brightness ratio in sprites [*Siefring et al.*, 2010]. The consequence of this is that strong optical emissions involving $N_2(B^3\Pi_g, v = 0)$ such as those at ~1046 nm and ~1231 nm corresponding to the N_2-1PG (0,0) and (0,1) bands will also produce significant differences among the NIR spectroscopic patterns of sprites, halos and sprite beads.

[10] The underlying microphysics explaining why the 1PG N_2 bead VDF ($v = 1$) is above its value at $v = 0$, 2 is connected to the fact that during the time (1.2 ms–2 ms) bead kinetics takes place, the population of $N_2(B^3\Pi_g, v = 1)$ remains above $N_2(B^3\Pi_g, v = 0)$ and $N_2(B^3\Pi_g, v = 2)$ by ~20% and ~5%, respectively. In sprite beads, electron-impact excitation is the most important production mechanism of $N_2(B^3\Pi_g, v)$. In particular, electron-impact excitation of $N_2(B^3\Pi_g, v = 1)$ is more efficient than that of $N_2(B^3\Pi_g, v = 0)$ even though radiative decay from $N_2(C^3\Pi_u, v = 0)$ to $N_2(B^3\Pi_g, v = 0)$ prevails over radiative decay from $N_2(C^3\Pi_u, v = 0)$ to $N_2(B^3\Pi_g, v = 1)$. Radiative decay from $N_2(C^3\Pi_u, v = 1)$ to $N_2(B^3\Pi_g, v = 0)$ and from $N_2(C^3\Pi_u, v = 2)$ to $N_2(B^3\Pi_g, v = 1)$ are less relevant. In the case of $N_2(B^3\Pi_g, v = 1)$, the intersystem collisional transfer (ICT) reaction $N_2(W^3\Delta_u, v = 1) + N_2 \rightarrow N_2(B^3\Pi_g, v = 1) + N_2$ [*Morrill and Benesch*, 1996] is the second largest process

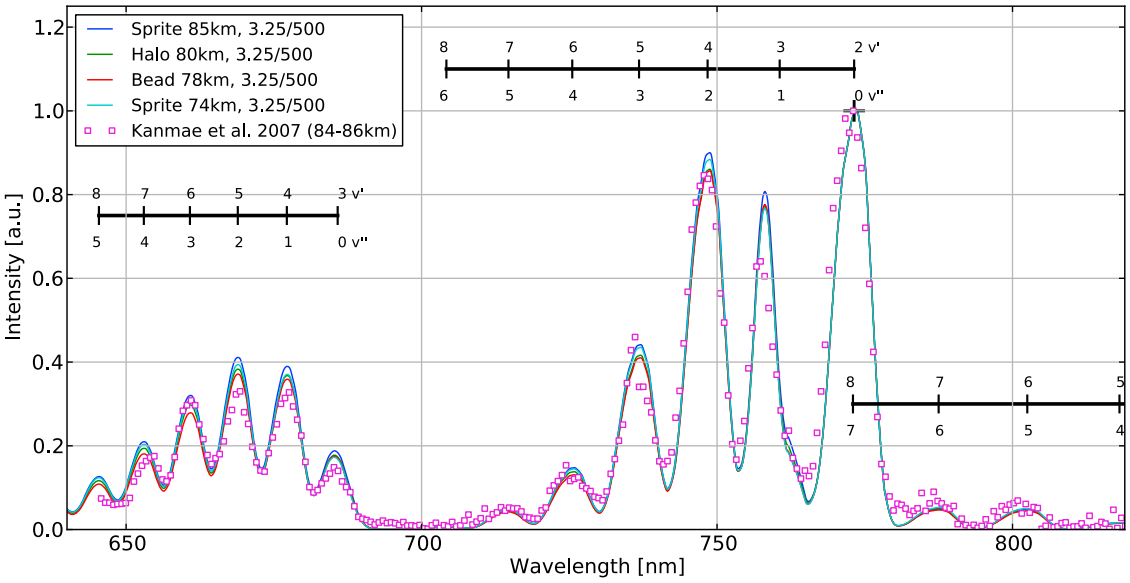

Figure 4. Modeled spectrum of the 1PG N_2 observed from a mountaintop at 3.25 km altitude and comparison with the observations by *Kanmae et al.* [2007].

producing $N_2(B^3\Pi_g, v = 1)$ only after electron-impact excitation and above radiative decays from $N_2(C^3\Pi_u, v = 0, 2)$.

[11] Recently, we proposed a simplified model [*Luque and Gordillo-Vázquez*, 2011b] that describes the VDF of the $N_2(B^3\Pi_g)$ depending on a single parameter w defined as the ratio of electron impact excitations of $N_2(C^3\Pi_u)$ to the combined electron impact excitations of $N_2(B^3\Pi_g)$ and $N_2(C^3\Pi_u)$. Roughly, w increases with higher dominant reduced electric fields. The shape of the 1PG N_2 VDFs shown in Figure 1a for bead, halos and sprites (at 74 km and 85 km) can be interpreted in the light of our simplified $N_2(B^3\Pi_g)$ VDF model. In particular, the VDF of beads plotted in Figure 1a corresponds to low values of w, where the different vibrational levels are populated mainly by direct impact electron excitation, whereas the VDF of sprites has a higher w, implying a more important role of radiative cascading from $N_2(C^3\Pi_u)$, which mostly populates the $v \leq 1$ levels of $N_2(B^3\Pi_g)$. Halos are an intermediate case between beads and sprites.

[12] The details of the shape between $v = 0$ and $v = 2$ of the 1PG N_2 VDFs shown in Figure 1a for bead, halos and sprites (at 74 km and 85 km) can be attributed, according to the detailed kinetic model, to the combination of three results. First, the VDF normalization, let's call it S, which is the sum of the time-integrated populations from $v = 2$ to $v = 6$ of $N_2(B^3\Pi_g)$, is such that $S_{bead} > S_{sprite} > S_{halo}$ with $S_{bead} \simeq 4.38\ S_{sprite}$ and $S_{sprite} \simeq 1.32\ S_{halo}$. Second, to the relative proportion between the calculated sprite-halo-bead time-integrated vibrational populations (see Table 1). Finally, as the third reason, we find that the vibrational populations decrease as we scale up in vibrational levels. The latter is fulfilled in sprites and halos though we found that in beads (as mentioned above) the population of $N_2(B^3\Pi_g, v = 1)$ remains above $N_2(B^3\Pi_g, v = 0)$ and $N_2(B^3\Pi_g, v = 2)$ due to the combination of a more efficient electron-impact excitation and the action of intersystem collisional transfer (ICT) reaction $N_2(W^3\Delta_u, v = 1) + N_2 \rightarrow N_2(B^3\Pi_g, v = 1) + N_2$ [*Morrill and Benesch*, 1996] producing $N_2(B^3\Pi_g, v = 1)$.

[13] Figure 1b shows that the $N_2(C^3\Pi_u)$ VDFs in sprites, halos and sprite beads clearly differ for $v = 0, 2$. For $v = 0$ the halos and sprite bead populations are 20% above that of sprites while for $v = 2$, sprite densities are 40%–50% above that of halos and sprite beads. For the less populated $v = 3, 4$ levels, the difference is less visible but still significant (sprite vibrational concentrations 2–3 times larger for $v = 3, 4$ than those of halos and beads).

[14] Due to the long optical slant path (between 300 km and 500 km) the signal from the TLEs can be strongly affected by absorption from various atmospheric constituents (O_2, H_2O, CO_2). To quantify this effect, we have estimated atmospheric transmittance using MODTRAN predictions [*Anderson et al.*, 1993] from the visible optical range up to 2000 nm where there is significant absorption due to water vapor. Figure 2 shows the transmittances of the 1PG $N_2(B^3\Pi_g)$ optical emissions from 640 nm to 2000 nm calculated assuming a 500 km atmospheric path length from mountain (3.25 km) [*Kanmae et al.*, 2007], airplane (14 km), balloon (35 km) and space platforms (full transmission), respectively, pointing to sprites (at 74 km and 85 km), halos (at 80 km) and sprite beads (at 78 km). For space observations, we assume an observer at 400 km altitude looking at the nadir corrected for atmospheric transmittance through 320 km atmospheric path lengths and neglecting absorption above 100 km altitude. The transmittances of the 2PG $N_2(C^3\Pi_u)$ optical emissions from 250 nm to 500 nm were calculated assuming a 300 km atmospheric path length from airplane (14 km) [*Heavner et al.*, 2010], balloon (35 km) and space (nadir view) platforms. It is clearly seen in Figure 2 that the important H_2O absorption in the NIR around 880 nm–980 nm and beyond 1000 nm is minimized when observing from aircrafts (14 km) and balloons (35 km). Similarly, the NUV - blue optical emissions from the 2PG $N_2(C^3\Pi_u)$ are better detected from high altitude planes [*Heavner et al.*, 2010] and above.

[15] The optical emission spectra of the 1PG N_2 from 640 nm to 1300 nm and 2PG N_2 from 250 nm to 500 nm

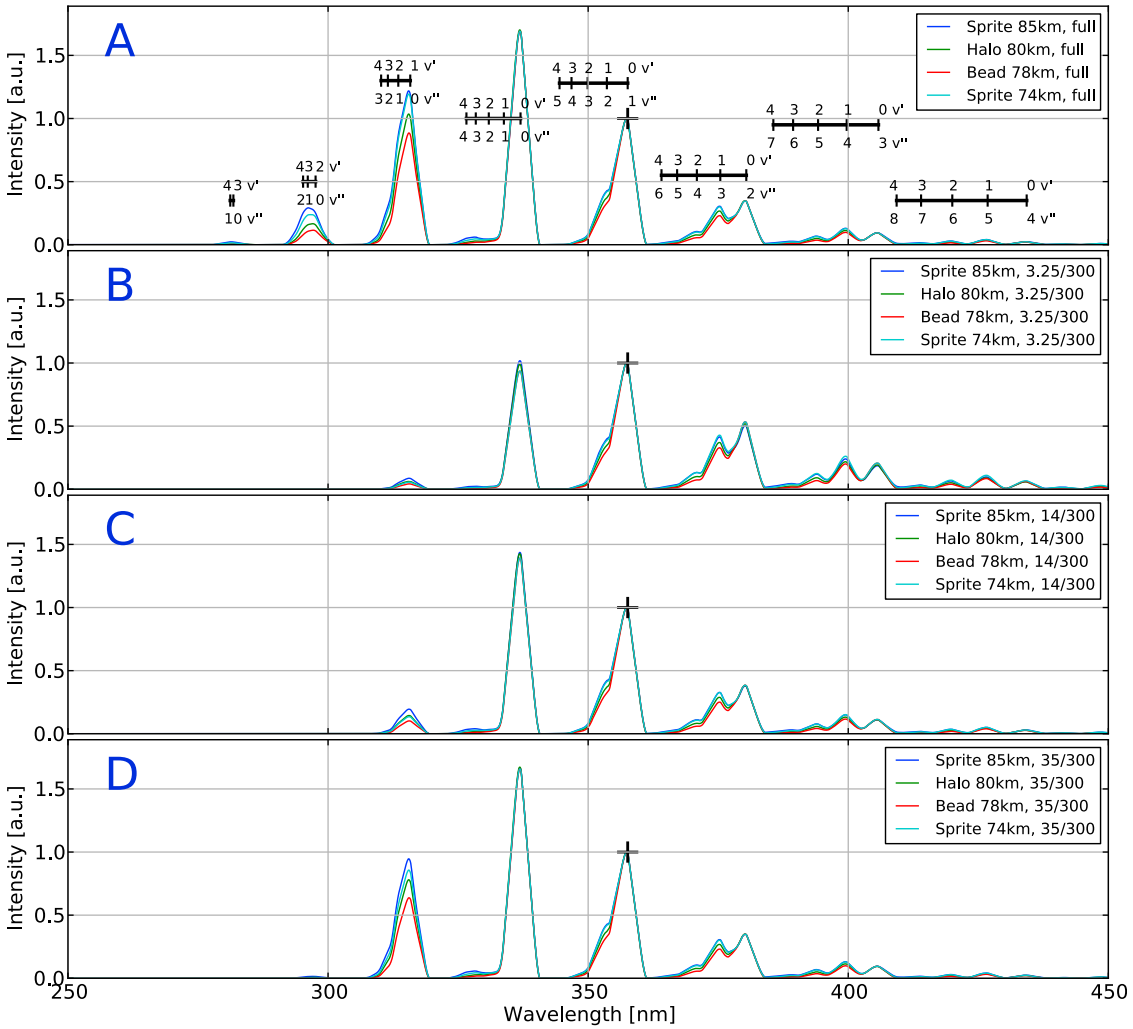

Figure 5. (a) Calculated spectra of the 2PG N_2 from 250 nm to 500 nm without correction for atmospheric transmittance, (b) corrected for atmospheric transmittance assuming 300 km atmospheric path length from observers in mountains (3.25 km), (c) airplanes (14 km), and (d) balloons (35 km). The spectrum from space (nadir) platforms at 400 km altitude is the same as that shown in Figure 5a. The spectra were calculated for a gas temperature of 220 K and a spectral resolution of $\Delta\lambda = 3.5$ nm. The normalization of the 2PG N_2 spectra was done with respect to the (0,1) transition at 357.6 nm. Note that the word *full* in Figure 5a stands for full transmittance.

are shown, respectively, in Figures 3 and 5 without correction for atmospheric transmittance (Figures 3a and 5a) and corrected for atmospheric transmittance assuming 500 km (for $N_2(B^3\Pi_g)$) and 300 km (for $N_2(C^3\Pi_u)$) atmospheric path lengths from observers in mountains (3.25 km, Figures 3b and 5b), airplanes (14 km, Figures 3c and 5c) and balloons (35 km, Figures 3d and 5d). The spectrum from space (nadir) platforms at 400 km altitude is the same as the spectra calculated assuming full light transmission, that is, without correction for atmospheric transmittance (see Figures 3a and 5a).

[16] The calculated band spectra of molecular nitrogen were multiplied by the atmospheric transmittance and convolved with a triangular slit function, of different full width at half maximum (FWHM), to produce the synthetic spectra at different spectral resolutions. In order to compare with available measured spectra, we have used a gas temperature of 220 K and spectral resolutions of $\Delta\lambda = 3$ nm [*Kanmae et al.*, 2007] and $\Delta\lambda = 3.5$ nm [*Heavner et al.*, 2010] for the synthetic spectra of the 1PG N_2 and 2PG N_2, respectively. In addition, the normalization point of the 1PG N_2 synthetic spectrum corresponds to the (2, 0) band at 773 nm, which is the same used in the experimentally recorded 1PG N_2 spectra by *Kanmae et al.* [2007]. The latter is important because, depending on the selection of the normalization point when comparing any two spectra, the observed spectral differences will be at different wavelengths. We see in Figure 3 that the spectra of sprites, halos and beads look the same between 640 nm and 880 nm, when normalized at 773.2 nm. However, what is most remarkable is that in the NIR region, there is a clear difference at $\simeq$1046 nm and $\simeq$1230 nm that can be up to a factor of two between the bead and sprite 1PG N_2 spectra (see Figure 3). Also, Figure 3 shows that the intensity of the NIR peaks are higher at 3.25 km than at 14 km, 35 km or space. The reason is that, according to the transmittance curves (see Figure 2), at

14 km (or 35 km) the relative light transmission at wavelengths higher than the one chosen for normalization (at 773.2 nm) of the 1PG N_2 spectrum is higher (because of the slope of the transmittance curve) for 3.25 km than for the case of 14 km and 35 km.

[17] For comparison, the sprite 1PG N_2 spectrum observed by *Kanmae et al.* [2007] is shown together with the calculated spectrum (for the same observational conditions set by *Kanmae et al.* [2007]) in Figure 3b and, with greater detail, in Figure 4, where a very good agreement is found. The 1PG N_2 synthetic spectrum exhibits distinct spectral features in the NIR region associated to sprites, halos and beads that, however, are not distinguished in the visible spectral range and that, because of their importance and relative values, we think could be detected from appropriate observation platforms.

[18] The synthetic 2PG N_2 spectra shown in Figure 5 were normalized with respect to the (0,1) transition at 357.6 nm and we used a spectral resolutions of $\Delta\lambda = 3.5$ nm similar to the one reported by *Heavner et al.* [2010] in the only 2PG N_2 spectrum recorded to date. The sequence of spectra in Figure 5 shows that the optical transitions associated to $v = 1, 2, 3, 4$ of the $C^3\Pi_u$ state clearly appear only when observing from sufficiently high altitudes (35 km and above) for which the sprite 2PG N_2 spectrum becomes 50% larger than the bead spectrum. A quantitative comparison between our calculated 2PG N_2 spectra shown in Figure 5 and the 2PG N_2 spectrum reported by *Heavner et al.* [2010] is not straightforward because *Heavner et al.* [2010] published their sprite $N_2(C^3\Pi_u)$ spectrum without correction for instrument spectral response.

4. Conclusions

[19] Near infrared (NIR) and ultraviolet (NUV) spectra of TLEs such as sprites, halos and sprite beads have been calculated for different scenarios of observation. Our calculations show that synthetic spectra of sprites, halos and sprite beads, when normalized to the (2,0) band at 773.2 nm, exhibit distinct spectroscopic features in the NIR region at $\simeq$1046 nm and $\simeq$1231 nm where sprite spectra are almost a factor of two more intense than that of sprite beads. The most remarkable difference between sprite and bead spectra is above electronic noise level and, consequently, we believe that it could be observable from planes, balloons and/or space platforms. Besides this, spectral differences of about 50% in some NUV bands originating from $v > 0$ levels of the $C^3\Pi_u$ state are also predicted between the spectroscopic fingerprints of sprites and beads. The visible region (640–820 nm) of our 1PG $N_2(B^3\Pi_g)$ synthetic spectra shows a very good agreement with the measurements by *Kanmae et al.* [2007]. Future dedicated campaigns for NIR and NUV spectroscopic measurements could confirm our present results concerning the unique spectroscopic features of sprites, halos and beads in the NIR region of the electromagnetic spectrum where one can find the most intense optical emissions of the studied TLEs.

[20] **Acknowledgments.** We thank T. Kanmae and H. C. Stenbaek-Nielsen for kindly providing their sprite spectrum data in the 640–820 nm spectral range of a sprite at 84.4–86.6 km recorded from Langmuir Laboratory. This work was supported by the Spanish Ministry of Science and Innovation, MICINN under projects AYA2009-14027-C05-02 and AYA2011-29936-C05-02 and by the Junta de Andalucia, Proyecto de Excelencia FQM-5965. A.L. was supported by a JAE-DOC contract partly funded by the European Social Fund (ESF).

[21] Robert Lysak thanks the reviewers for their assistance in evaluating this paper.

References

Anderson, G. P., et al. (1993), MODTRAN2: Suitability for remote sensing, *Proc. SPIE Int. Soc. Opt. Eng.*, *1968*, 514.

Barrington-Leigh, C. P., U. S. Inan, and M. Stanley (2001), Identification of sprites and elves with intensified video and broadband array photometry, *J. Geophys. Res.*, *106*, 1741, doi:10.1029/2000JA000073.

Bucsela, E., J. Morrill, M. Heavner, C. Siefring, S. Berg, D. Hampton, D. Moudry, E. Wescott, and D. Sentman (2003), N2($B^3\prod_g$) and $N_2^+(A^2\prod_u)$ vibrational distributions observed in sprites, *J. Atmos. Sol. Terr. Phys.*, *65*, 583, doi:10.1016/S1364-6826(02)00316-4.

Gilmore, F. R., R. R. Laher, and P. J. Espy (1992), Franck-Condon factors, r-centroids, electronic transition moments, and Einstein coefficients for many nitrogen and oxygen band systems, *J. Phys. Chem. Ref. Data Monogr.*, *21*, 1005, doi:10.1063/1.555910.

Gordillo-Vázquez, F. J. (2008), Air plasma kinetics under the influence of sprites, *J. Phys. D*, *41*(23), 234016, doi:10.1088/0022-3727/41/23/234016.

Gordillo-Vázquez, F. J. (2010), Vibrational kinetics of air plasmas induced by sprites, *J. Geophys. Res.*, *115*, A00E25, doi:10.1029/2009JA014688.

Gordillo-Vázquez, F. J., and A. Luque (2010), Electrical conductivity in sprite streamer channels, *Geophys. Res. Lett.*, *37*, L16809, doi:10.1029/2010GL044349.

Gordillo-Vázquez, F. J., A. Luque, and M. Simek (2011), Spectrum of sprite halos, *J. Geophys. Res.*, *116*, A09319, doi:10.1029/2011JA016652.

Hampton, D. L., M. J. Heavner, E. M. Wescott, and D. D. Sentman (1996), Optical spectral characteristics of sprites, *Geophys. Res. Lett.*, *23*, 89, doi:10.1029/95GL03587.

Heavner, M. J., J. S. Morrill, C. Siefring, D. D. Sentman, D. R. Moudry, E. M. Wescott, and E. J. Bucsela (2010), Near-ultraviolet and blue spectral observations of sprites in the 320–460 nm region: N_2 (2PG) emissions, *J. Geophys. Res.*, *115*, A00E44, doi:10.1029/2009JA014858.

Kanmae, T., H. C. Stenbaek-Nielsen, and M. G. McHarg (2007), Altitude resolved sprite spectra with 3 ms temporal resolution, *Geophys. Res. Lett.*, *34*, L07810, doi:10.1029/2006GL028608.

Luque, A., and U. Ebert (2009), Emergence of sprite streamers from screening-ionization waves in the lower ionosphere, *Nat. Geosci.*, *2*, 757, doi:10.1038/ngeo662.

Luque, A., and U. Ebert (2010), Sprites in varying air density: Charge conservation, glowing negative trails and changing velocity, *Geophys. Res. Lett.*, *37*, L06806, doi:10.1029/2009GL041982.

Luque, A., and F. J. Gordillo-Vázquez (2011a), Sprite beads originating from inhomogeneities in the mesospheric electron density, *Geophys. Res. Lett.*, *38*, L04808, doi:10.1029/2010GL046403.

Luque, A., and F. J. Gordillo-Vázquez (2011b), Modeling and analysis of N2($B^3\prod_g$) and $N_2(C^3\prod_u)$ vibrational distributions in sprites, *J. Geophys. Res.*, *116*, A02306, doi:10.1029/2010JA015952.

Luque, A., and F. J. Gordillo-Vázquez (2012), Mesospheric electric breakdown and delayed sprite ignition caused by electron detachment, *Nat. Geosci.*, *5*, 22, doi:doi:10.1038/ngeo1314.

Mende, S. B., R. L. Rairden, G. R. Swenson, and W. A. Lyons (1995), Sprite spectra; N_2 1 PG band identification, *Geophys. Res. Lett.*, *22*, 2633, doi:10.1029/95GL02827.

Morrill, J. S., and W. M. Benesch (1996), Auroral N_2 emissions and the effect of collisional processes on N_2 triplet state vibrational populations, *J. Geophys. Res.*, *101*, 261, doi:10.1029/95JA02835.

Morrill, J. S., E. J. Bucsela, V. P. Pasko, S. L. Berg, M. J. Heavner, D. R. Moudry, W. M. Benesch, E. M. Wescott, and D. D. Sentman (1998), Time resolved N_2 triplet state vibrational populations and emissions associated with red sprites, *J. Atmos. Sol. Terr. Phys.*, *60*, 811, doi:10.1016/S1364-6826(98)00031-5.

Siefring, C. L., J. S. Morrill, D. D. Sentman, and M. J. Heavner (2010), Simultaneous near-infrared and visible observations of sprites and acoustic-gravity waves during the EXL98 campaign, *J. Geophys. Res.*, *115*, A00E57, doi:10.1029/2009JA014862.

Simek, M. (2002), The modelling of streamer-induced emission in atmospheric pressure, pulsed positive corona discharge: N_2 second positive and NO-γ systems, *J. Phys. D*, *35*, 1967, doi:10.1088/0022-3727/35/16/311.

Simek, M., G. Dilecce, and S. DeBenedictis (1995), On the use of the numerical simulation of the first positive system of N_2: 1. Emission and LIF analysis, *Plasma Chem. Plasma Process.*, *15*(3), 427.

Wescott, E. M., H. C. Stenbaek-Nielsen, D. D. Sentman, M. J. Heavner, D. R. Moudry, and F. T. S. Sabbas (2001), Triangulation of sprites, associated halos and their possible relation to causative lightning and micrometeors, *J. Geophys. Res.*, *106*, 10,467, doi:10.1029/2000JA000182.